A first principles systematic study of the structural, electronic, and magnetic properties of Heusler X₂MnZ with X=Fe, Co, Ni, Cu, Ru, Rh, Pd, Ag, Pt, Au and Z=Al, Si, Ga, Ge, In and Sn.

A first principles systematic study of the structural, electronic, and magnetic properties of Heusler X_2MnZ with X=Fe, Co, Ni, Cu, Ru, Rh, Pd, Ag, Pt, Au and Z=Al, Si, Ga, Ge, In and Sn.

F. Aguilera-Granja[1] and R.H. Aguilera-del-Toro[1] and J. L. Morán-López[2]

[1]*Instituto de Física, Universidad Autónoma de San Luis Potosí, San Luis Potosí, México*[*]

[2]*División de Materiales Avanzados, Instituto Potosino de Investigación Científica y Tecnológica, San Luis Potosí, México*[†]

(Dated: May 17, 2019)

Abstract

An exhaustive study of the structural stability, electronic, and magnetic properties of the ternary X_2MnZ Heusler alloys, in cubic and tetragonal lattice cells, is presented. We performed density-functional-theory (DFT) calculations, as implemented in the SIESTA code, for X=Fe, Co, Ni, Cu, Ru, Rh, Pd, Ag, Pt, and Au, and Z=Al, Si, Ga, Ge, In, and Sn. To optimize the crystal structure and the lattice constants a local relaxation by means of the conjugate algorithm is used. The spin polarized local electronic density of states for the different chemical components in the various alloys are calculated and some particular examples are discussed. From those results we observe that the alloys that show half-metallic behaviour are Fe_2MnSi, Co_2MnSi, and Co_2MnGe. A general feature is that Mn donates of the order of one electron to the other components. We calculated the magnetic moment per unit cell and the individual contributions coming from all the components, and observe the change as a function of X and Z. The largest moment per unit cell corresponds to Fe_2MnIn (7.86 μ_B) and the smallest to Ru_2MnIn (2.15 μ_B). We compared our results with the existing experimental data for the lattice constants and the magnetic moments per unit cell and found a fair agreement.

Keywords: DFT calculations, structure, electronic, and energetic properties, Heusler alloys

INTRODUCTION

Heusler alloys (HA) are some of the most interesting magnetic systems. They are ternary alloys with a chemical formula X_2MnZ, that crystallize with a $L2_1$ structure [1–7]. This structure can be described by four interpenetrating *fcc* sublattices; two of them occupied by the X atoms, and the other two by Mn and the Z element. In general, the X element is a transition or noble metal and Z is one element of the IIIA (Al, Ga, In), IVA (Si, Ge, Sn) or VA (Sb) columns of the periodic table.

As can be observed in Figure 1, in the structural ground state, the Mn atoms (light brown circles) are surrounded by eight first neighbors of type X (pink circles) and six second neighbors of type Z (blue circles). Thus, the shortest Mn-Mn pair occurs at the third neighbor shell. Due to the large distance between Mn atoms, it is believed that the magnetic coupling is via the itinerant electrons of the X atoms, and the Z element contributes to the size of the lattice parameter. At finite temperatures, when the atoms exchange lattice sites, the magnetic interactions, sign and magnitude, are determined by the amount of spatial disorder present in the system i.e., how many first, second and third Mn neighbors pairs exists at that temperature.

In all the HA, Mn plays an important role and depending on the chemical composition and the atomic order, they can be ferromagnets, ferrimagnets, antiferromagnets of various types, or helicoidal. In the case in which the X component is non-magnetic the magnetic

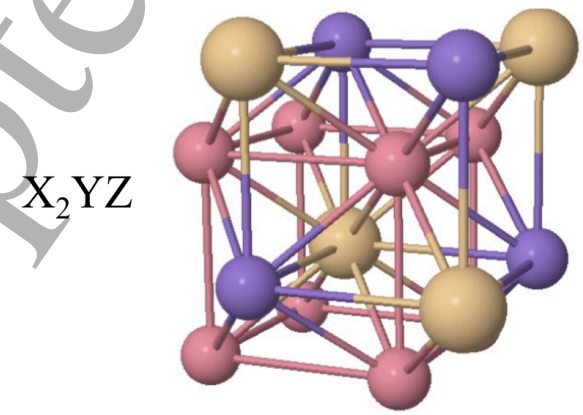

FIG. 1. (Color online) The X_2MnZ unit cell used in the electronic structure calculation. The Mn atoms are denoted by light brown circles, the X element (Co, Fe, Ni, Cu, Ru, Rh, Pd, Ag, Pt, Au) by pink circles and the Z atom (Al, Si, Ga, Ge, In, and Sn) by blue circles.

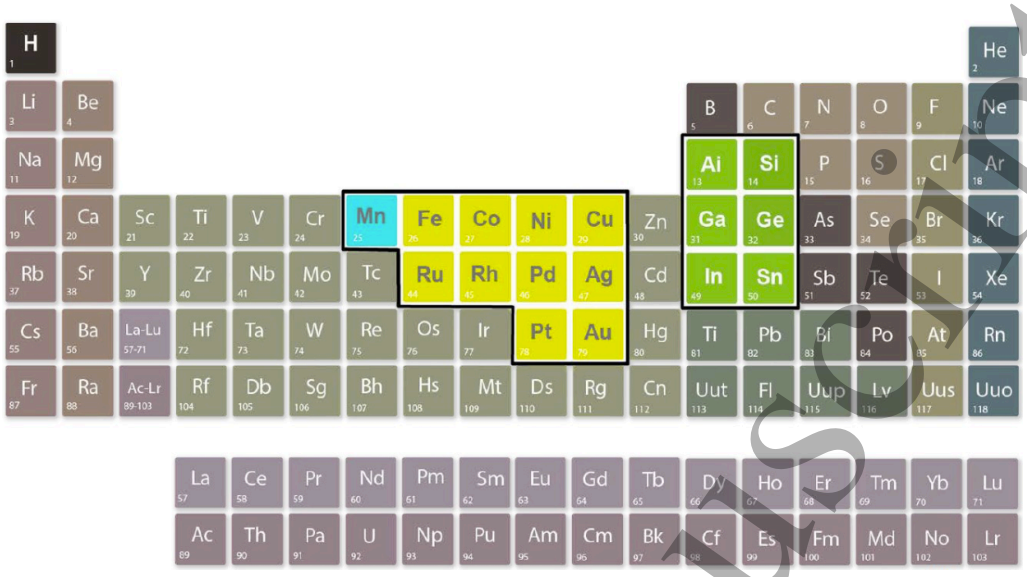

FIG. 2. (Color online) Positions that occupy the chemical elements X, Mn, and Z, in the Periodic Table, constituting the Heusler alloys studied here. The X are highlighted in yellow and Z elements in green.

moment is mainly localized in the Mn atom and the total magnetization per unit cell can be as high as 4.4 μ_B (Pd_2MnAl)[3]. On the other hand, if X is magnetic, both magnetic elements can give rise to 5.11 μ_B per unit cell (Co_2MnGe)[3]. Furthermore, HA show Curie temperatures that can be as high as 985 K (Co_2MnSi)[3].

As a function of temperature, the three chemical spices exchange lattice sites and produce a rich variety of atomic disordered systems that influence the magnetic properties. These alloys present a great opportunity to understand the interplay between magnetism and atomic order[8, 9]. In addition, in some systems, like Ni-Mn-Ga, the coupling between structure and magnetism, induce martensitic transformations that produce interesting magnetic shape-memory and magnetic superelasticity properties[10].

One more property that makes these systems subject of intensive research is that some are half-metallic. There is a gap in the minority spin sub-band at the Fermi level. Thus, they can be used to provide electrons with only one spin polarization; the key property for spintronics [11, 12] and magnetically driven actuators[13].

From the theoretical point of view, the electronic and magnetic structure of particular HA have been studied by means of several theoretical approaches. Non self-consistent spherical augmented plane wave methods (SAPW) were used by Ishida et al. to study Cu_2MnAl

[14], and later Co_2MnSn[15]. Kübler et al.[16] studied Co_2MnAl, Co_2MnSn, Ni_2MnSn, Pd_2MnIn, Pd_2MnSn, Cu_2MnAl, and Cu_2MnSn by means of the augmented spherical wave (ASW) framework within the local spin density (LSD) treatment of exchange and correlation. The case of Ni_2MnGa was analyzed by means of the linear muffin-tin orbital (LMTO) method within the LSD approximation[17]. By means of full-potential linearized augmented plane-wave (FLAPW) method, based on the density functional theory (DFT) within the generalized gradient approximation (GGA) for exchange and correlation, Ayuela et al.[18] reported results on Co_2MnGa, Ni_2MnAl, Ni_2MnGa, and Ni_2MnSn, Deb and Sakurai[19] reported results on Cu_2MnAl, and Kulkova et al.[20, 21] studied Co_2MnGa, Ni_2MnGa, and Cu_2MnAl. The local spin density pseudopotential plane wave approach was used by Godlevsky and Rabe[22] to study Ni_2MnGa. Furthermore, to estimate the interatomic exchange interactions and the Curie temperatures of Ni_2MnZ, with Z=Ga, In, Sn and Sb, Şaşioğlu et al.[23] used the augmented spherical wave (ASW) method within the atomic-sphere approximation.

Our interest here is to study in a systematic way, the lattice stability, the electronic and magnetic properties of 60 systems; i.e. X=Fe, Co, Ni, Cu, Ru, Rh, Pd, Ag, Pt, and Au, and Z = Al, Ga, In, Si, Ga, and Sn. This report represents the most complete set of HA up to date. We present in Figure 2, the periodic table showing the elements that form the X_2MnZ systems reported here: Mn, the transition metals in yellow (X element) and the IIIA and IVA column elements in green (Z element).

In Section II we present the model and computational details. In Sec. III we discuss our results; first we address ground state crystalline structure then we discuss the electronic structure and the magnetic properties of the various HA series. A comparison with other theoretical studies and the experimental results is also given. Finally, our conclusions are contained in Sec. IV.

DETAILS OF THE COMPUTATIONAL PROCEDURE AND MODEL

Our calculations were performed using the SIESTA DFT package[24], which employs numerical pseudo-atomic orbitals as basis sets to solve the single-particle Kohn-Sham equations. In this work we used the Perdew-Burke-Ernzerhof form of the generalized gradient approximation (GGA) for the exchange and correlation potential[25], and the

atomic cores were described by nonlocal norm-conserving scalar-relativistic Troullier-Martins pseudopotentials[26], factorized in the Kleinman-Bylander form[27]. The pseudo-potentials for all the different elements studied here, were generated using the valence configurations. More details on the reliability, basis sets used, and about the pertinent tests that we carried out, can be found in the literature[28, 29]. The valence states were described using a double-ζ doubly polarized basis set.

An electronic temperature of 25 meV for smearing, and a 250 Ry energy cutoff to define the real-space grid for numerical calculations involving the electron density was used. We have tested larger cutoffs and lower electronic temperatures for some particular cases, and verified that they do not modify substantially the results. To optimize the lattice constant and atomic positions we performed a local relaxation using the conjugate gradient algorithm[30], starting from cubic and tetragonal basic lattice cells. The structural optimization was finalized when each force component, on each atom in the basic cell, was smaller than 6 meV/Å.

All the calculations were performed assuming cubic and tetragonal lattice vectors with a supercell of 16 atoms, which is four times the unit formula, (see Figure 1) keeping the X_2MnZ stoichiometry. The binding energy E_b is defined as follows:

$$E_b(X_8Mn_4Z_4) = \frac{E_{\rm Total}(X_8Mn_4Z_4) - 8E_{\rm atom}(X) - 4E_{\rm atom}(Mn) - 4E_{\rm atom}(Z)}{16}. \quad (1)$$

RESULTS

We calculated the electronic structure of the 60 systems; X_2MnZ with X=Fe, Co, Ni, Cu, Ru, Rh, Pd, Ag, Pt and Au and Z = Al, Ga, In, Si, Ga, and Sn. We included in the calculation all the s, p, and d, valence electrons. Through a self-consisting procedure we obtained the ground state crystallographic structure, cubic or orthorombic, and the equilibrium lattice constants. We present in detail the spin-polarized, up and down, local electronic density of states (SPLDS) for some representative systems, in the energy region around the Fermi energy. We show also how the total spin up and down electronic densities of states evolve as we substitute for a particular X series, the Z element.

The physical properties are discussed in three tables for each series X=3d, 4d, and Pt, and the noble metals. First, we give the cohesive energy of the alloys and the equilibrium

TABLE I. Structural properties of the X_2MnZ Heusler alloys. The X element is a magnetic $3d$ element, and Z = Al, Ga, In, Si, Ge, and Sn. The crystalline structure for all the systems is cubic. The lattice constant is given in (Å), and the binding energy in eV/atom.

X_2MnZ	Calculated Lattice Parameter ($\AA$)	Experimental Lattice Parameter ($\AA$)	Binding Energy (eV/atom)
Fe_2MnAl	5.909		-4.288
Fe_2MnGa	6.006		-3.956
Fe_2MnIn	6.197		-3.659
Fe_2MnSi	5.651	5.664[31]	-4.767
Fe_2MnGe	5.789		-4.385
Fe_2MnSn	6.142		-3.990
Co_2MnAl	5.789, 5.68[16]	5.756[3]	-4.736
Co_2MnGa	5.873, 5.723[18], 5.726 [20]	5.770[3]	-4.347
Co_2MnIn	6.078		-3.988
Co_2MnSi	5.694	5.654[3]	-5.080
Co_2MnGe	5.825	5.743[3]	-4.772
Co_2MnSn	6.066, 5.95[16],	6.000[3]	-4.382
Ni_2MnAl	5.909, 5.793[18], 5.782 [22]		-4.477
Ni_2MnGa	5.993, 5.85[17], 5.808[18], 5.771[22], 5.811[20]	5.825[6]	-4.131
Ni_2MnIn	6.162 5.988[22]	6.068[3]	-3.811
Ni_2MnSi	5.766		-4.664
Ni_2MnGe	5.909	5.76[32]	-4.429
Ni_2MnSn	6.138, 5.99[16], 6.057[18]	6.052[3]	-4.111

crystalline structures and lattice constants. Then, we note how the electrons distribute in the ordered alloy and from the local electronic density of states we analyze the half-metallic behavior. Finally, from the spin-polarized density of states, we calculate the magnetic moment at each chemical component, and the total magnetic moment per unit cell.

X_2MnZ with X = Fe, Co, Ni, and Z = Al, Ga, In, Si, Ga, and Sn

The theoretical values, for the lattice parameter in Å,calculated by different methods and approximations, and the reported experimental values are given in Table I, columns 2 and 3. The cohesive energy in eV, is given in the last column. In the Fe series, the smallest lattice parameter, and the highest cohesive energy, for the elements in Column IIIA, of the periodic table, corresponds to Al, 5.909 Å and 4.288 eV, respectively. On the other hand, the largest lattice parameter and the smallest cohesive energy of the elements in that column is attained in the In case, 6.197 Å and 3.659 eV, respectively. For the elements in the IVA

TABLE II. Transferred electronic charge between the atoms of the X_2MnZ Heusler like systems with X = Fe, Co, Ni and Z= Al, Ga, In Si, Ge and Sn. In the last column the calculated band gap in the spin-down band of the half-metallic systems is given.

X_2YZ	X(Charge) (e)	Mn(Charge) (e)	Z(Charge) (e)	spin down band gap (eV)
Fe_2MnAl	0.473	-0.899	-0.048	
Fe_2MnGa	0.510	-0.674	-0.346	
Fe_2MnIn	1.030	-0.784	-1.276	
Fe_2MnSi	1.035	-0.706	-1.365	0.66
Fe_2MnGe	0.815	-0.846	-0.784	
Fe_2MnSn	1.024	-0.693	-1.354	
Co_2MnAl	0.348	-0.944	0.250	
Co_2MnGa	0.317	-0.723	0.090	
Co_2MnIn	0.941	-0.851	-1.030	
Co_2MnSi	0.705	-0.731	-0.678	0.69
Co_2MnGe	0.407	-0.949	0.136	0.58
Co_2MnSn	0.957	-0.765	-1.148	
Ni_2MnAl	0.315	-1.036	0.407	
Ni_2MnGa	0.177	-0.895	0.540	
Ni_2MnIn	0.814	-1.024	-0.603	
Ni_2MnSi	0.600	-0.859	-0.341	
Ni_2MnGe	0.199	-1.063	0.664	
Ni_2MnSn	0.884	-0.881	-0.886	

column a similar trend is observed: the smallest and largest lattice constants and the highest and smallest cohesive energy correspond to Si and Sn. In this series the experimental value reported by Niculescu et al.[31] for Fe_2MnSi, differs with our result only by 0.013 Å.

The Co series is the most studied, experimentally and theoretically. With the exception of the In system, there are experimental results[3] for the rest. In general the calculated values are in very good agreement with the measurements. The experimental value for Z=Al is 5.756 Å. Our result is 5.789 Å and the reported value by Kübler et al.[16] is 5.68 Å. For Z=Ga the experimental values is 5.77 Å. Our calculation gives 5.873 Å, and other results reported by Ayuela et al.[18] and Kulkova et al.[20], are 5.723 , and 5.726 Å, respectively. For Z=Si and Ge the experimental values are 5.654 and 5.743 Å, and we obtained 5.694 and 5.825 Å, respectively. For Z=Sn the experimental value is 6 Å. Our result is 6.066 and the value published by Kübler et al.[16] is 5.95 Å. In regards with our calculation the largest discrepancy corresponds to Co_2MnGa (0.103 Å).

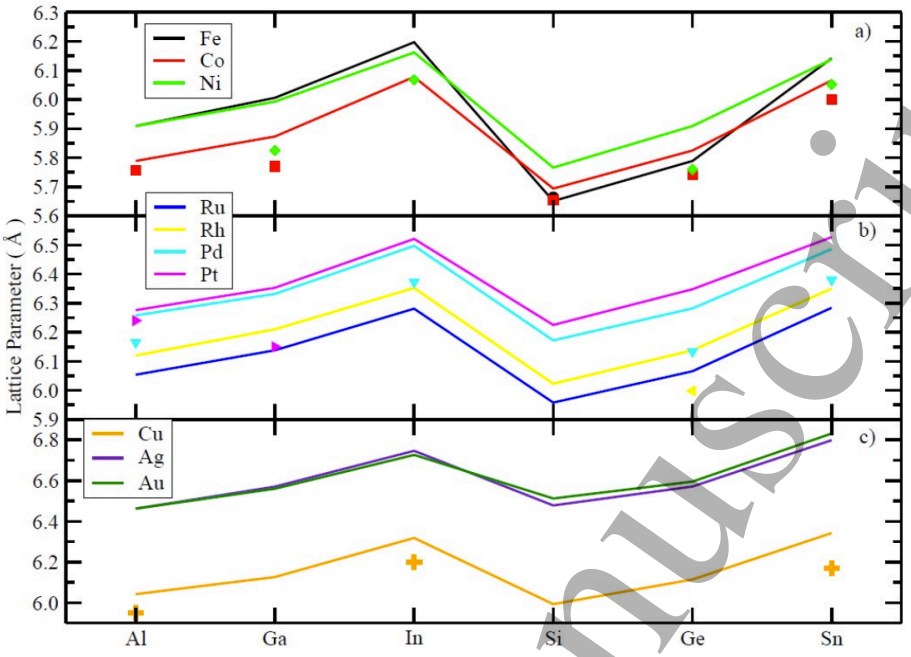

FIG. 3. (Color online) The lattice parameter dependence on Z for the X_2MnZ. In Fig. a) X is a 3*d* transition metal, in Fig. b) X is a 4*d* transition metal and Pt, and in c) X=Cu, Au ,and Ag. The experimental results are shown with symbols of the same color.

The Ni Heusler alloys that have been analysed experimentally are those with Ga, In, Ge, and Sn. The calculated (experimental) values for the lattice constants, all in angstroms, are 5.993 (5.825), 6.162 (6.008), 5.909 (5.76), and 6.138 (6.052), respectively. Other calculations are also given for comparison in the same column. In this series, the most studied system is Ni_2MnGa. The reported values are: 5.85[17], 5.808[18], 5.771[22], and 5.811[20].

To obtain a clearer picture of how the lattice parameter depends on the element Z, we show in Figure 3 the results for the lattice parameters. In the upper part, the results for the 3*d* series are displayed. The black, red, and green lines correspond to the Fe, Co, and Ni series, respectively. The reported experimental measurements are also plotted. In the case of Fe_2MnZ, the lattice constant for Z=Si is shown by a black circle. The results for the Co series are marked by red squares. In the Ni case there are experimental results for Z=Ga, In, Ge, and Sn and are shown by green diamonds.

In Table II, we summarize the electron distribution in the three atomic components of the 3*d* magnetic series. In the second to fourth columns, we give the difference between the total number of electrons of each element in the atomic case minus that number when they are alloyed. For the case of Fe series, Mn and the Z atoms donate electrons to Fe. In the

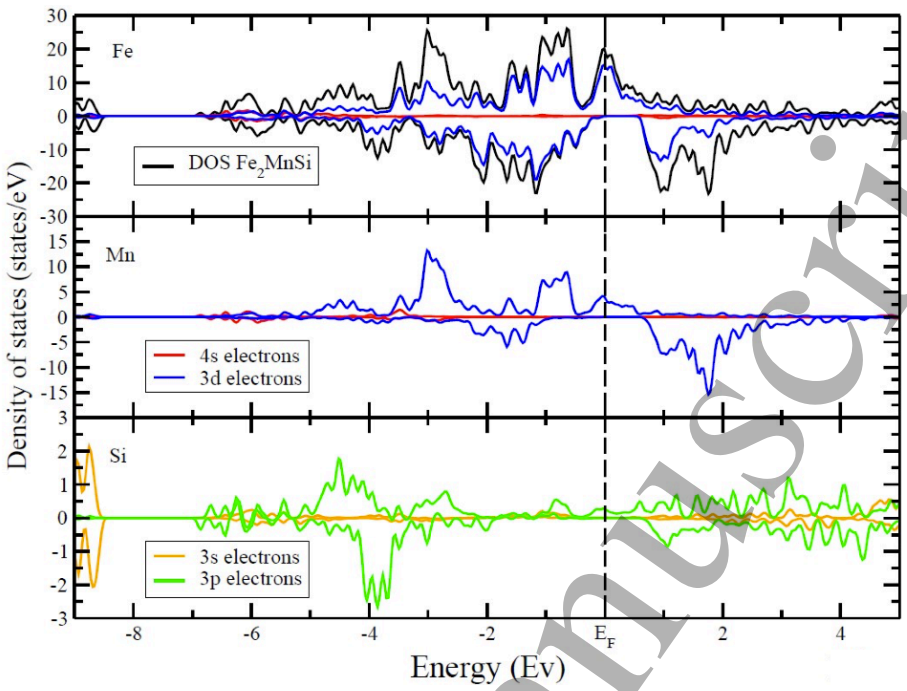

FIG. 4. (Color online) Electronic spin polarized local density of states (SPLDS) for the Fe_2MnSi alloy. In the upper panel the total spin polarized densities of states (black line) and the 3*d* Iron contribution (purple line) are shown. In the central panel the electronic structures at the Mn atoms are preented; the 3*d* (in blue), and the 4*s* (in red). In the bottom panel, the Si electronic structure is shown; the 3*p* (in green) and the 3*s* (in light brown). Notice that the lower panel has a different vertical scale.

Co and Ni series the behavior is similar except for Z= Al, Ga, and Ge, cases in which the Z element receives electrons. The magnetic elements Fe, Co, and Ni always increase their number of electrons, reducing thereby their atomic magnetic moment, as will be commented below. The smallest charge transfer from Mn occurs in Fe_2MnGa (0.674 electrons), and the largest in Ni_2MnAl (0.899 electrons).

In the last column we present the value of the calculated gap in the minority spin electronic sub-band. In all the series there are only three half-metallic alloys: Fe_2MnSi, Co_2MnSi, and Co_2MnGe. The corresponding sub-band gaps have a width of 0.66, 0.69, and 0.53 eV, respectively. A finite gap in the spin-down sub-band allows to extract electrons with a single polarization, with potential applications as spin valves. The system with the highest electron density of states, at the Fermi energy, for spin-up electrons corresponds to the Fe alloy.

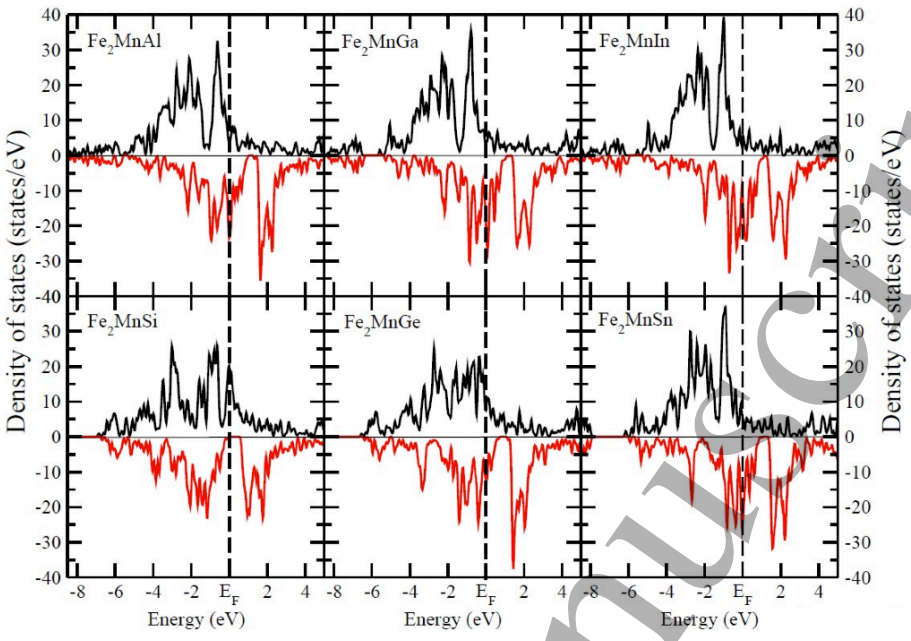

FIG. 5. (Color online) Total electronic spin polarized local density of states for the six Fe systems Z=Al, Si, Ga, Ge, In, and Sn.

In Figure 4 we show the results for the spin-polarized local density of states (SPLDS) for Fe_2MnSi alloy, on each of the chemical elements. It is important to note that the vertical scales are different in the three panels. In the upper panel we present the total spin-polarized electronic density of states (black curve), and the $3d$ (in blue), $4s$ (in red), Fe electronic contributions. In the central panel we show the SPLDS on the Mn sites. One sees that the $3d$ electron sub-band with spin down is mostly empty, giving rise to a large magnetic moment. In the lower one the $3s$ (in yellow) and $3p$ (in green) contribution from the Si atoms are shown. As reported previously, we observe that the $3d$ electrons of Fe and Mn are the ones that determine the magnetic properties of the system. The $4s$ electrons form a wide conducting band. On the other hand, the Si spectrum shows a wide $3p$ band partially polarized and a $3s$ band, deep in energy. One more characteristic of this system is the gap of 0.66 eV in the spin-down SPLDS at the Fermi energy, which gives the half-metallic character of this alloy[12]. It is also important to note that the local density of states at the Fermi level are the $3d$ Fe electrons.

In Figure 5, we show the electronic structure of the six systems Fe_2MnZ; Z=Al, Ga, and In, in the upper figures and Si, Ge, and Sn, in the lower part. In the IIIA elements (upper panel) the density of states look very similar; the Fermi level falls in $3d$ electron populated

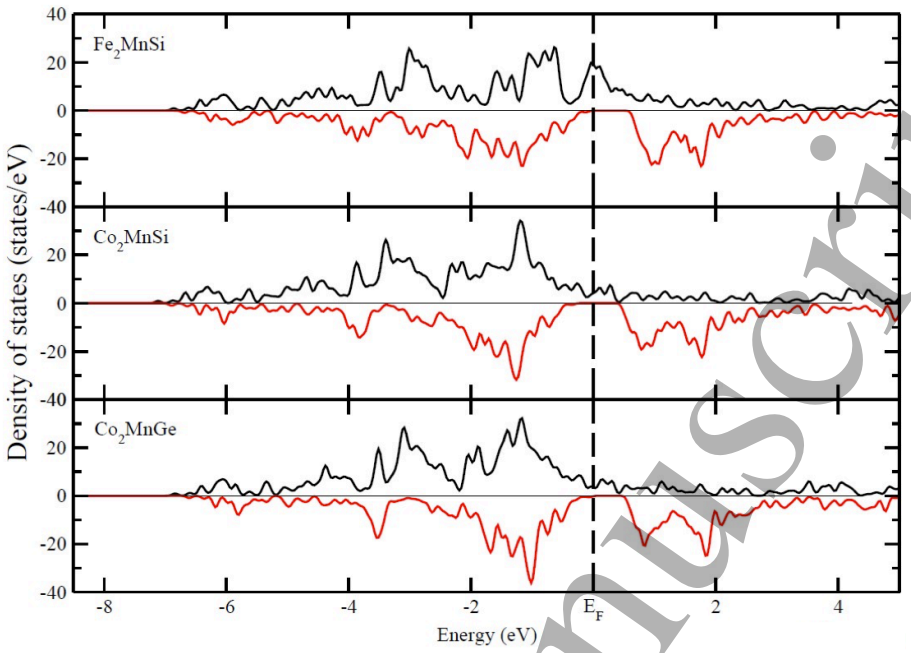

FIG. 6. (Color online) Total electronic spin polarized local density of states for the three half-metallic alloys Fe_2MnSi, Co_2MnSi, and Co_2MnGe.

regions, and the Mn spin down density of states in mostly empty. There is a valley in the spin down band but it is some electronvolts above E_F. In the IVA elements, we see that the general characteristics around the Fermi energy prevail, i.e. the $3d$ electrons from Fe and Mn are the most important but the value in the spin-down density of states at E_F is zero in the Si system. For Ge and Sn this gap moves above E_F. Also, as mentioned above, a general behavior is the donation of electrons from the Mn atoms to the Fe atoms.

In Figure 6 we show the results for the SPLDS for the three half-metallic systems Fe_2MnSi, Co−2MnSi, and Co_2MnGe. We see that the Fe alloy has an important peak in the spin-up density of states produced by the Mn-Fe $3d$ electron hybridization. This characteristic offers the possibility for obtaining a high polarized electronic current and makes this alloy a good candidate for spintronic applications. The Co alloys, Z=Si and Ge, show band gaps 0.69 and 0.58 eV, respectively, but the value of the spin-up density of states, at E_F, is much smaller that in the case of Fe.

In Table III, we show the results for the magnetic moment per unit cell and the contributions coming from the three chemical elements. In the second and third column we present the theoretical and experimental magnetic moment per unit cell values, respectively. It is worth noticing that most of the experimental values are reported at high temperatures, situ-

TABLE III. The magnetic moment per unit cell (μ_B), and the magnetic moments of each of the elements in the X_2MnZ Heusler alloys. The X element is a magnetic $3d$ element, and Z = Al, Ga, In, Si, Ge, and Sn. Other reported theoretical values are also given in column two. The available experimental data is presented in column three.

X_2MnZ	Theor. Mag. Mom./ (per unit cell)(μ_B)	Exp. Mag. Mom./ (per unit cell) (μ_B)	X (μ_B)	Mn (μ_B)	Z (μ_B)
Fe_2MnAl	6.40		2.193	2.413	-0.400
Fe_2MnGa	7.22		2.374	2.828	-0.362
Fe_2MnIn	7.86		2.428	3.134	-0.130
Fe_2MnSi	3.00	2.2[31]	0.081	2.828	0.010
Fe_2MnGe	4.91		1.325	2.502	-0.242
Fe_2MnSn	7.10		2.118	3.043	-0.178
Co_2MnAl	4.07, 4.05[16]	4.01[3]	0.612	3.066	-0.226
Co_2MnGa	4.21, 4.08[18], 4.09[20]	4.05[3]	0.605	3.229	-0.230
Co_2MnIn	4.97		0.799	3.415	-0.046
Co_2MnSi	5.00	5.07[3]	0.893	3.253	-0.037
Co_2MnGe	5.00	5.11[3]	0.901	3.395	-0.196
Co_2MnSn	5.09, 5.02[16]	5.08[3]	0.817	3.491	-0.038
Ni_2MnAl	4.28, 4.03[18], 4,22[22]	4.19[7]	0.304	3.742	-0.019
Ni_2MnGa	4.33, 4.17[17], 4.09[18], 4.05[21], 4.22[22]	4.17[3]	0.299	3.871	-0.138
Ni_2MnIn	4.45, 4.31[22]	4.40[3]	0.244	3.942	0.020
Ni_2MnSi	4.07		0.178	3.665	0.045
Ni_2MnGe	4.17		0.217	3.845	-0.106
Ni_2MnSn	4.29, 3.75[16], 4.08[18]	4.05[3]	0.176	3.897	0.036

ation in which there may be a considerable amount of chemical disorder. Thus, since all the calculated values are at zero temperature, and perfect chemical order, a direct comparison is not possible. At finite temperatures the magnetic and chemical disorder may modify the magnitude of the magnetic moments[8].

The highest and lowest values, for the magnetic moment per unit cell, are obtained for the Fe series. The highest magnetic moment per unit cell corresponds to Fe_2MnIn, which is 7.86 μ_B. The partial contributions for Fe, Mn and In are 2.428, 3.13 and -0.130 μ_B, respectively. On the other hand, the lowest value occurs in Fe_2MnSi which is 3 μ_B per unit cell. The partial values are 0.081, 2.828 and 0.010 μ_B for Fe, Mn, and Si, respectively. In this case there are some experiments that report the properties in a chemically disordered state [31]. The authors report values of 1.35 and 2.2 μ_B, per unit cell, at 77 and 4.2 K, respectively. For comparison with the theoretical calculation, we take the value measured

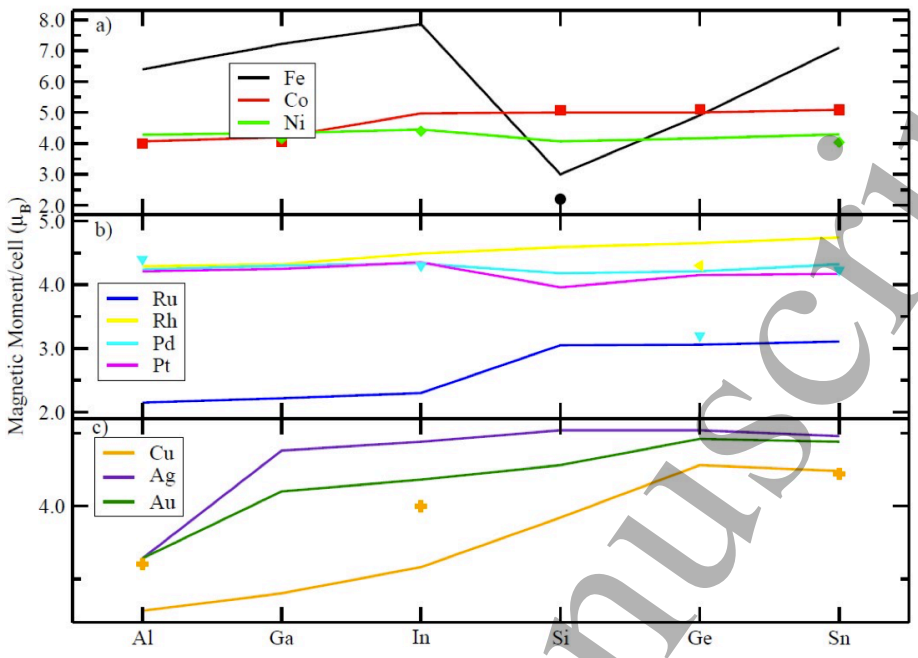

FIG. 7. (Color online) The magnetic moment per cell dependence on the Z element for X_2MnZ. Fig. a) corresponds to the case where X is a 3*d* transition metal, b) to the case where X is a 4*d* transition metal and Pt, and c) to the case where X=Cu, Au ,and Ag. The experimental results are shown with symbols of the same color.

at the lowest temperature. It is also important to note that the coupling of Mn with the Z element, except for the case of Si, is antiferromagnetic.

As mentioned above, the Co series is the most studied and experimental results for five out of the six cases are reported. The largest value for the magnetic moment per unit cell ($5.09\mu_B$) is obtained for Co_2MnSn which is in very good agreement with the experimental value (5.08 μ_B). The theoretical partial values for the magnetic moment are 0.817 (Co), 3.491 (Mn) and -0.038 (Sn) μ_B. In the other cases the theoretical and experimental values are in very good agreement. In the second column we show also the theoretical results obtained within other theoretical models. The reported values in the case of Z=Al, are 5.02[16], 5.06[15], for Z=Ga, 4.08[18], 4.09[20], and for Z=Sn, 5.02[16], 5.06[15]. We observe that the magnetic coupling between Mn and the Z elements is antiferromagnetic in all cases.

In the Ni series the largest value for the magnetic moment per unit cell corresponds to Ni_2MnIn (4.45 μ_B), a value very similar to the one reported experimentally (4.40 μ_B). Manganese shows also the largest magnetic moment value (3.942 μ_B) of the 3*d* alloys. The other three cases reported experimentally, Ni_2MnAl, Ni_2MnGa and Ni_2MnSn, differ more

TABLE IV. Structural properties of the X_2MnZ Heusler alloys. X is an element of the 4*d* series, and Pt, and Z = Al, Ga, In, Si, Ge, and Sn. The crystalline structure are cubic or tetragonal. In column two, the theoretical values calculated by different methods and approximations, are given. In the case of tetragonal lattices, the average value, is also given. In column three the reported experimental values are included.

X_2MnZ	Theoretical Lattice Parameter (Å)	Experimental Lattice Parameter (Å)	Binding Energy (eV/atom)
Ru_2MnAl	6.054		-5.475
Ru_2MnGa	6.138		-5.052
Ru_2MnIn	6.281		-4.751
Ru_2MnSi	5.958		-5.842
Ru_2MnGe	6.066		-5.516
Ru_2MnSn	6.284		-5.143
Rh_2MnAl	6.120		-5.298
Rh_2MnGa	6.210		-4.897
Rh_2MnIn	6.352		-4.660
Rh_2MnSi	6.023		-5.470
Rh_2MnGe	6.138	5.998[4]	-5.207
Rh_2MnSn	6.350		-4.965
Pd_2MnAl	2×6.343, 6.088		-4.182
	6.258	6.165[3]	
Pd_2MnGa	2×6.430, 6.138		-3.856
	6.332		
Pd_2MnIn	2×6.612, 6.268		-3.635
	6.497, 6.13 [16]	6.373[3]	
Pd_2MnSi	2×6.194, 6.129		-4.202
	6.172		
Pd_2MnGe	6.282	6.134[5]	-4.050
Pd_2MnSn	6.486, 6.35[16]	6.380[3]	-3.864
Pt_2MnAl	2×6.505, 5.817		-5.286
	6.276	6.24[4]	
Pt_2MnGa	2×6.594, 5.872		-4.865
	6.337	6.16[4]	
Pt_2MnIn	2×6.820, 5.923		-4.649
	6.524		
Pt_2MnSi	2×6.561, 5.552		-5.208
	6.224		
Pt_2MnGe	2×6.690, 5.665		-5.004
	6.348		
Pt_2MnSn	2×6.887, 5.806		-4.834
	6.527		

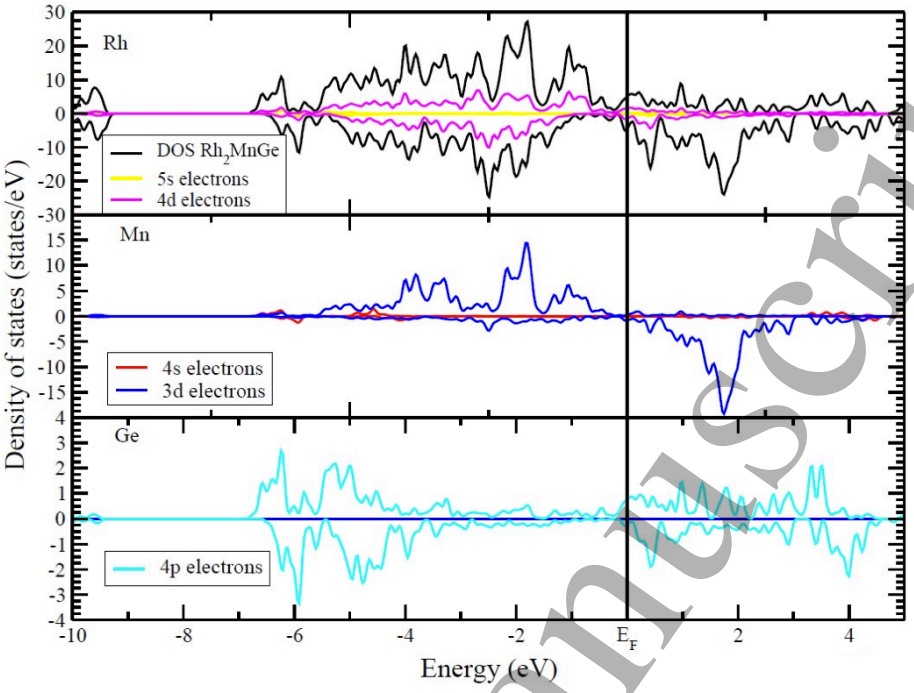

FIG. 8. (Color online) Electronic spin polarized local density of states (SPLDS) for the Rh_2MnAl alloy. In the upper panel, the total spin polarized densities of states (black line) and the $3d$ Rhodium contribution (purple line), are shown. In the central panel, the electronic structures at the Mn atoms, are presented ; the $3d$ (in blue), and the $4s$ (in red). In the bottom panel, the Ge $4p$ (in light blue) electronic structure is shown. Notice that the lower panel has a different vertical scale.

from our ground state (zero K) calculations. For these series In, Si, and Sn couple ferromagnetically to the other two chemical elements. That is not the case of Z= Al, Ga, and Ge, whose coupling is antiferromagnetic. The most studied system is Ni_2MnGa, for which the published theoretical results are: 4.17[17], 4.09[18], 4.05[21], 4.22[22] μ_B.

We show in Figure 7 a) the calculated results for the $3d$ systems and compare them to the experimental values. The Fe, Co, and Ni results are shown by black, red and green curves, and the experimental results are shown by symbols of the same color. One observes that in the case of the Fe series, there are two lines, for the IIIA and IVA elements. The strong reduction in the Si alloy is produced by an important reduction of the Fe magnetic moment (0.081 μ_B). In the case of Co, we observe a small increase in the IIIA elements and an almost constant value for the IVA elements. In the case of Ni, there is also a small increase in the IIIA elements followed by a decrease in the Si alloy to increase from that point to Sn.

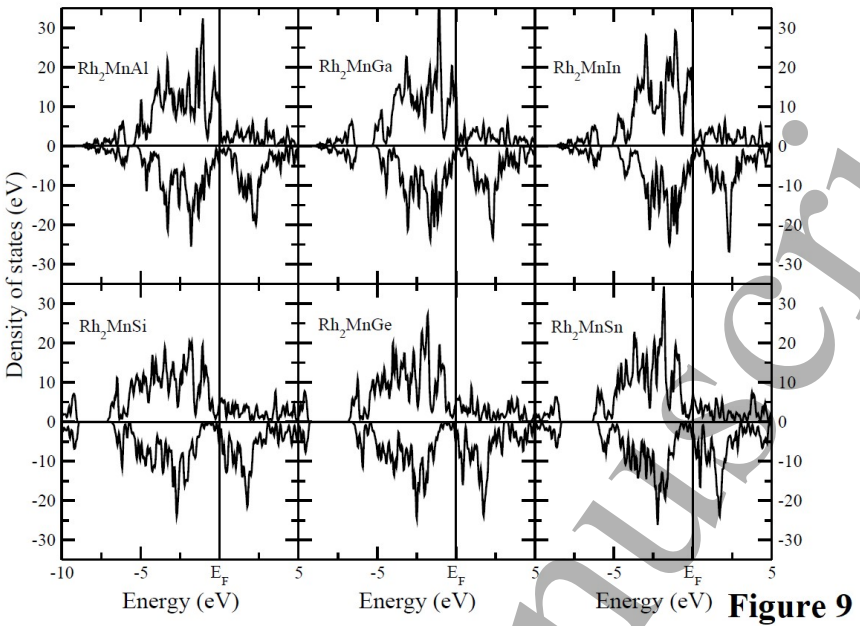

Figure 9

FIG. 9. Total electronic spin polarized local density of states for the six Rh systems Z=Al, Si, Ga, Ge, In, and Sn.

The reduction in the Si case is also producd by a reduction of the Ni magnetic moment. In general, we can consider a very good agreement between theory and experiment.

X_2MnZ with X = Ru, Rh, Pd, Pt, and Z = Al, Ga, In, Si, Ga, and Sn

Now we consider the series of $4d$ elements and $5d$ Pt. In Table IV, we give the results for the lattice parameter in Å and the cohesive energy in eV. The Ru, and Rh series are all cubic. In the Pd series, four cases are tetragonal (Z=Al, Ga, In, and Si). All the six Pt systems are tetragonal. In the Table, for the tetragonal lattices, we give the dimensions of the base and hight of the cell and the average in the row bellow. In the same column we give other published theoretical results. It is worth noticing that only the case Pd_2MnIn and Pd_2MnSn, Kübler et al. reported the values 6.13 and 6.35 Å, respectively. In the third row we present the available experimental results. Our theoretical results differ from the experimental values for amounts that go from 0.5 to 2.8% . The cases that we can compare to, are those that are ferromagnetic (Rh_2MnGe, Pd_2MnGe, and Pd_2MnSn). As discussed below, it has been found that in the alloys Pd_2MnAl, Pd_2MnIn, Pt_2MnAl, and Pt_2MnGa, the Mn atoms couple antiferromagnetically among themselves.

In Figure 3 b) we show how the lattice constants changes for the 4*d* and Pt series as a function of the Z element. In this case the Z element dependence is similar for the four series Ru, Rh, Pd and Pt. The lines are almost parallel. The smaller lattice constants and the cohesive energy correspond to the Ru alloys and the larger ones to the Pt alloys. For the Ru alloys there are no experimental results. In the case of the Rh alloys only the Rh_2MnGe has been studied. The experimental lattice constant is 5.998 Å and the one calculated is 6.138 Å. Several systems of the Pd series have been measured: Z=Al, In, Ge, and Sn. These values are shown by blue inverted triangles. In the case of the Pt series, the cases of Z=Al and Ga have been measured. These experimental results are shown by magenta triangles.

In Figure 8 we show the results for the spin-polarized local density of states (SPLDS) for the Rh_2MnGe alloy, on each of the chemical elements, with $L2_1$ crystallographic structure. It is worth noticing that the vertical scale is different in the three panels. In the upper panel we present the total SPLDS (black curve), and the 4*d* (in purple) Rh electronic contribution. In this case the band spin splitting is small and one expects a reduced magnetic moment. In the central panel we show the SPLDS on the Mn sites. One sees that the 3*d* electron band with spin down is mostly empty, giving rise to an important contribution to the alloy magnetic moment. In the lower figure, the Ge electronic contribution is presented; the 4*s* and 3*d* bands are completely full and deeper in energy. The only valence electrons are the 4*p* (in green) states.

As mentioned above the 4*d* Rh spin-up and spin-down sub-bands appear with similar occupation and we observe that the 3*d* electrons of Mn are the ones that determine the magnetic properties of the system. The 4*s* electrons form a wide conducting band. On the other hand, the Ge spectrum shows a wide 4*p* band partially polarized.

In Figure 9 we show how the electronic structure changes as the Z element goes from Al to In (Group IIIA) and from Si to Sn (Group IVA). The spin-down sub-band bellow the Fermi energy, is mainly produced by the X element whereas the spin-down sub-band above the Fermi energy comes from the 3*d* Mn electrons. One further observation is that there is a valley close to the E_F but the gap in the spin-down band observed for X=Co and Z=Si and Ge is not present in these series. A similar behavior is obtained for X=Ru, Pd, and Pt, but the electronic valley is below E_F.

In Table V, we summarize the electron distribution in the three atomic components of the 4*d* series and the 5*d* Pt. In the second to fourth columns, we give the difference between

TABLE V. Transferred electronic charges between the atoms of the X_2MnZ Heusler like systems with X = Ru, Rh, Pd, Pt and Z= Al, Ga, In, Si, Ge and Sn.

X_2YZ	X(Charge) (e)	Mn(Charge) (e)	Z(Charge) (e)
Ru_2MnAl	0.767	-1.125	-0.411
Ru_2MnGa	0.893	-0.980	-0.807
Ru_2MnIn	1.406	-0.930	-1.881
Ru_2MnSi	1.189	-0.701	-1.677
Ru_2MnGe	1.026	-1.086	-0.965
Ru_2MnSn	1.321	-0.913	-1.728
Rh_2MnAl	0.697	-1.160	-0.233
Rh_2MnGa	0.800	-1.100	-0.500
Rh_2MnIn	1.283	-1.060	-1.507
Rh_2MnSi	1.031	-0.819	-1.241
Rh_2MnGe	0.826	-1.113	-0.538
Rh_2MnSn	1.208	-0.943	-1.475
Pd_2MnAl	0.332	-1.032	0.369
Pd_2MnGa	0.358	-1.100	0.383
Pd_2MnIn	0.840	-1.081	-0.598
Pd_2MnSi	0.575	-0.915	-0.233
Pd_2MnGe	0.226	-1.069	0.619
Pd_2MnSn	0.816	-0.906	-0.726
Pt_2MnAl	0.354	-1.156	0.448
Pt_2MnGa	0.433	-1.175	0.310
Pt_2MnIn	0.971	-1.182	-0.761
Pt_2MnSi	0.610	-0.940	-0.281
Pt_2MnGe	0.338	-1.119	0.443
Pt_2MnSn	0.944	-1.010	-0.880

the total number of electrons of each element in the atomic case minus that number when they are alloyed. In all the cases, electrons are transferred to the X elements (Ru, Rh, Pd, and Pt). The Mn atoms donate electrons as much as 1.182, in the case of Pt_2MnIn, but in most of the cases the transfer is about 1 electron. The Z element acts also as a donor for the Ru and Rh. In the other two series (Pd and Pt) and in the cases of Z=Al, Ga, and Ge, the Z element behaves as an acceptor of electrons. On the other hand, for Z=In, Si, and Sn these elements are donors.

In Table VI, we show the results for the magnetic moment per unit cell and the contributions coming from the three chemical elements. Our results and those published by other authors are given in column two. In the cases where experimental values are reported, we

TABLE VI. Magnetic moment per unit cell (μ_B), and the magnetic moments of each of the elements in the X_2MnZ Heusler alloys. The X component is a $4d$ element and Pt, and Z = Al, Ga, In, Si, Ge, and Sn. Other reported theoretical values are also given in column 2. The available experimental data is presented in column three.

X_2MnZ	Theo. Mag. Mom./ per unit cell(μ_B)	Exp. Mag. Mom./ per unit cell(μ_B)	X(μ_B)	Mn(μ_B)	Z(μ_B)
Ru_2MnAl	2.15		-0.379	2.868	0.039
Ru_2MnGa	2.22		-0.433	3.092	-0.011
Ru_2MnIn	2.30		-0.526	3.328	0.021
Ru_2MnSi	3.05		-0.089	3.191	0.039
Ru_2MnGe	3.06		-0.134	3.316	0.013
Ru_2MnSn	3.11		-0.229	3.483	0.086
Rh_2MnAl	4.29		0.237	3.860	-0.037
Rh_2MnGa	4.32		0.222	3.960	-0.080
Rh_2MnIn	4.49		0.211	4.090	-0.015
Rh_2MnSi	4.59		0.335	3.907	0.017
Rh_2MnGe	4.65	4.30[4]	0.348	3.995	-0.038
Rh_2MnSn	4.74		0.310	4.075	0.039
Pd_2MnAl	4.24	4.40[3]	0.059	4.150	-0.023
Pd_2MnGa	4.30		0.084	4.242	-0.109
Pd_2MnIn	4.33	4.30[3]	0.043	4.303	-0.053
Pd_2MnSi	4.18		0.054	4.096	-0.024
Pd_2MnGe	4.21	3.2[5]	0.076	4.181	-0.115
Pd_2MnSn	4.32, 3.86[16]	4.23[3]	0.032	4.246	0.008
Pt_2MnAl	4.21		0.090	4.051	-0.018
Pt_2MnGa	4.25		0.105	4.121	-0.084
Pt_2MnIn	4.35		0.087	4.220	-0.049
Pt_2MnSi	3.96		0.048	3.924	-0.063
Pt_2MnGe	4.15		0.086	4.065	-0.083
Pt_2MnSn	4.17		0.040	4.128	-0.042

show them in column three. In the Ru series, this element couples antiferromagnetically to Mn, but the Z elements couple ferromagnetically to give rise to magnetic moments per unit cell that goes from 2.15 to 3.11 μ_B. In the Rh, Pd, and Pt series the X elements and Mn contribute positively to produce magnetic moments per unit cell in the range of 3.96 (Pt_2MnSi) to 4.74 (Rh_2MnSn) μ_B.

The systems that have been studied experimentally are Rh_2MnGe, Pd_2MnAl, Pd_2MnIn, Pd_2MnGe, and Pd_2MnSn. The calculated (experimental) values are: 4.65 (4.30[4]), 4.24 (4.4[3]), 4.33 (4.3[3]), 4.21 (3.2[5]) and 4.32 (4.23[3]), all in μ_B. For the last system Kübler

TABLE VII. Structural properties of the X_2MnZ Heusler alloys. The X element is a noble metal, and Z = Al, Ga, In, Si, Ge, and Sn. The crystalline structure are cubic or tetragonal. The lattice constant is given in (Å), and the binding energy in eV/atom. In column two, the theoretical values calculated by different methods and approximations are given In the case of tetragonal lattices, the average value is also given. In column three, the reported experimental values, are included.

X_2MnZ	Theoretical Lattice Parameter (Å)	Experimental Lattice Parameter (Å)	Binding Energy (eV/Atom)
Cu_2MnAl	6.042, 5.85[16], 5.947[20]	5.950[3], 5.949[2]	-3.527
Cu_2MnGa	6.126		-3.224
Cu_2MnIn	6.318	6.206[2]	-2.990
Cu_2MnSi	5.993		-3.574
Cu_2MnGe	6.114		-3.437
Cu_2MnSn	6.342, 6.13[16]	6.173[2]	-3.189
Ag_2MnAl	6.462		-2.898
Ag_2MnGa	6.570		-2.657
Ag_2MnIn	6.746		-2.501
Ag_2MnSi	6.478		-2.875
Ag_2MnGe	6.571		-2.826
Ag_2MnSn	6.798		-2.672
Au_2MnAl	6.462	6.36[2]	-3.371
Au_2MnGa	6.560		-3.059
Au_2MnIn	6.726		-2.888
Au_2MnSi	6.512		-3.250
Au_2MnGe	6.594		-3.211
Au_2MnSn	6.831		-3.026

et al. also estimated a magnetic moment of 3.86 μ_B [16].

The results for the magnetic moment per atomic cell as a function of the element Z, are shown in Fig. 7 b). The Ru series is plotted in blue and acquires the lowest values, between 2.15 and 3.11 μ_B. One differentiates clearly two almost constant plateaux; one for the IIIA elements around 2 μ_B and other for the IVA elements near to 3 μ_B. The results for X=Pt (purple line), Pd (light blue), and Rh (light yellow) are very similar for the IIIA elements with values in the range of 4.21 and 4.49 μ_B. For the IVA elements there are some differences; in the Pt family there is a small decrease for Z=Si, and the it increases from 3.96 to 4.17 μ_B. In the case of the Pd alloys, the values are very similar to the IIIA group. Finally for Rh the values for the IVA elements increase their magnetic moment further up to 4.74 μ_B for Z=Sn.

TABLE VIII. Transferred electronic charges between the atoms of the X_2MnZ Heusler like systems with X = Cu, Ag, Au, and Z= Al, Ga, In Si, Ge and Sn

X_2MnZ	X(Charge) (e)	Mn(Charge) (e)	Z(Charge) (e)
Cu_2MnAl	0.297	-1.031	0.437
Cu_2MnGa	0.217	-1.001	0.568
Cu_2MnIn	0.730	-1.216	-0.245
Cu_2MnSi	0.468	-1.029	0.095
Cu_2MnGe	0.132	-1.068	0.804
Cu_2MnSn	0.764	-1.015	-0.514
Ag_2MnAl	0.278	-1.042	0.486
Ag_2MnGa	0.295	-1.142	0.553
Ag_2MnIn	0.617	-1.235	0.000
Ag_2MnSi	0.367	-1.105	0.372
Ag_2MnGe	0.177	-1.063	0.709
Ag_2MnSn	0.585	-1.013	-0.157
Au_2MnAl	-0.0885	-0.949	1.126
Au_2MnGa	-0.1237	-1.026	1.272
Au_2MnIn	0.032	-1.092	1.029
Au_2MnSi	0.011	-1.041	1.018
Au_2MnGe	-0.103	-0.999	1.206
Au_2MnSn	0.284	-1.019	0.452

It is important to recall that these results are obtained with an atomic base of 16 atoms, and all the Mn atoms are coupled ferromagnetically. In the reported literature, the Mn magnetic moment in Rh_2MnGe, Pd_2MnGe, and Pd_2MnSn, couple ferromagnetically but in Pd_2MnAl, Pd_2MnIn, Pt_2MnAl, and Pt_2MnGa they couple antiferromagnetically. The antiferromagnetic systems must be studied with a large enough atomic cell to be able to describe the three different types of antiferromagnetism characteristic of Heusler alloys. In the ferromagnetic cases the agreement between theory and experiment are very good, except for the case of Pd_2MnGe, in which the calculated magnetic moment is 4.21 μ_B and the one measured[5] is 3.2 μ_B

X_2MnZ with X = Cu, Ag, Au, and Z = Al, Ga, In, Si, Ga, and Sn

The cases in which the X element is a noble metal, X= Cu, Ag and Au are discussed now. In Table VII we present the results for the crystalline structure, lattice parameters, and the cohesive energy. The ground state crystalline structure in all the systems is cubic,

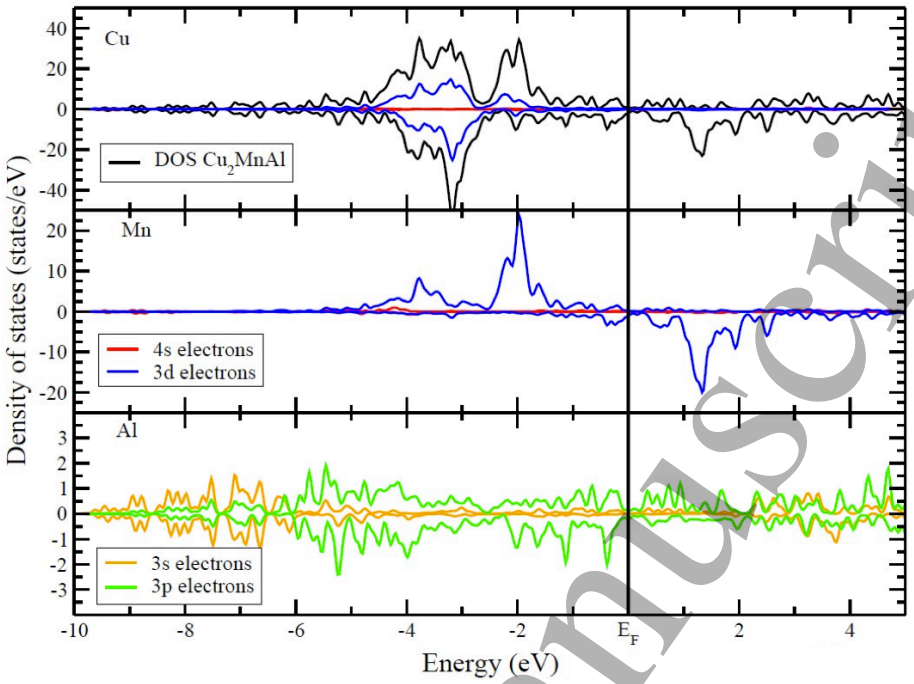

FIG. 10. (Color online) Electronic spin polarized local density of states (SPLDS) for the Cu_2MnAl alloy. In the upper panel, the total spin polarized densities of states (black line) and the 3*d* Copper contribution (purple line), are shown. In the central panel, the electronic structures at the Mn atoms is presented; the 3*d* (in blue), and the 4*s* (in red). In the bottom panel, the Al electronic structure is shown; the 3*p* (in green) and the 3*s* (in light brown). Notice that the lower panel has a different vertical scale.

but in the Au series, the tetragonal structures are very close in energy. Our results as well as other reported calculations are given in column 2. One can observe that the calculated lattice parameter and the measured values in Cu systems (Z=Al, In, and Sn), are in very fair agreement with our calculation. The most studied case is Cu_2MnAl: the theoretical values are 6.042 (this report), 5.85[16], 5.947[20] and the measured values 5.950[3], 5.949[2].

In the case of X=Ag, there are neither experimental nor previous theoretical studies reported. Finally for X=Au, only the case of Au_2MnAl was analysed experimentally. Our result differs by only 0.1 Å.

We present in Figure 3 c) the Z dependence of the lattice parameter for the noble elements Cu, Ag and Au. The smaller values correspond to the Cu series. Furthermore, the Ag and Au, Z dependence is very similar. The largest unit cell of all the systems reported here corresponds to Au_2MnSn (6.83 Å). The systems synthesized up to now are X=Cu, Z=Al,

TABLE IX. Magnetic moment per unit cell (μ_B), and the magnetic moments of each of the elements in the X_2MnZ Heusler alloys. The X element is a noble metal, and Z = Al, Ga, In, Si, Ge, and Sn. Other reported theoretical values are also given in column 2. The available experimental data is presented in column three.

X_2MnZ	Theo. Mag. Mom./ per unit cell (μ_B)	Exp. Mag. Mom./ per unit cell (μ_B)	X(μ_B)	Mn(μ_B)	Z(μ_B)
Cu_2MnAl	3.64, 3.38[16], 3.20[19], 3.47[20]	3.80[3] 4.12[2]	-0.031	3.803	-0.103
Cu_2MnGa	3.70		-0.020	3.933	-0.200
Cu_2MnIn	3.79	3.95[2]	-0.080	4.050	-0.094
Cu_2MnSi	3.96		-0.020	3.899	0.095
Cu_2MnGe	4.14		0.046	4.058	-0.010
Cu_2MnSn	4.12, 3.61[16]	4.11[2]	-0.032	4.097	0.088
Ag_2MnAl	3.82		-0.058	4.084	-0.148
Ag_2MnGa	4.19		0.011	4.302	-0.129
Ag_2MnIn	4.22		-0.021	4.393	-0.132
Ag_2MnSi	4.26		-0.009	4.259	0.014
Ag_2MnGe	4.26		0.033	4.271	-0.081
Ag_2MnSn	4.24		-0.056	4.332	0.024
Au_2MnAl	3.82	2.24[2]	-0.013	4.043	-0.200
Au_2MnGa	4.05		0.029	4.210	-0.222
Au_2MnIn	4.09		0.004	4.324	-0.237
Au_2MnSi	4.14		0.024	4.206	-0.113
Au_2MnGe	4.23		0.051	4.253	-0.126
Au_2MnSn	4.22		-0.016	4.349	-0.102

In, and Sn, and X=Au, Z=Al.

In Figure 10 we present the total SPLDS and the individual SPLDS for the case Cu_2MnAl. In the upper figure, we see that the Cu d sub-bands are completely filled (blue curve). In contrast, as seen in the middle figure, the spin-down Mn sub-band is mostly empty, and as we will discuss bellow, it gives rise to the magnetic properties of the alloy (see black curve in the upper panel). The Al densities of states are presented in the lower panel. Here, again the electron occupancy in spin-up and spin-down sub-bands are also very similar and do not contribute significantly to the total magnetic moment. The $3s$ and $3p$ electrons only contribute to the electron conductivity.

In Figure 11, the total spin polarised densities of states for up- and down-spin of the six Cu-alloys are shown. The general behavior for the six alloys is very similar to the Al-case. The Cu d sub-bands (up and down) are filled. In the systems with Z belonging to the IIIA

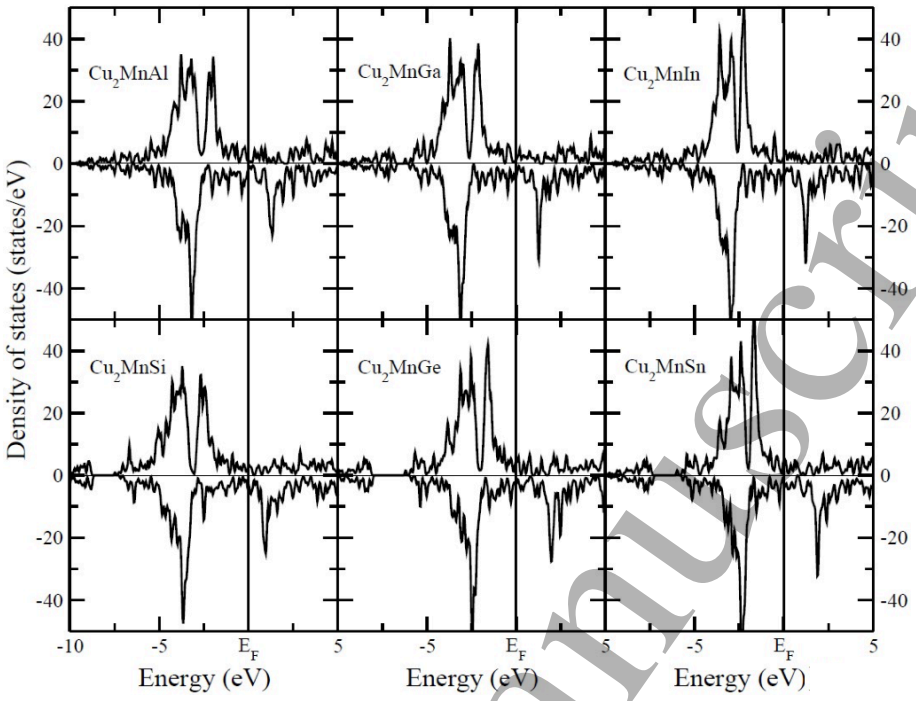

FIG. 11. Total electronic spin polarized total local density of states for the six Cu systems Z=Al, Si, Ga, Ge, In, and Sn.

column (Al, Ga, and In) a week hybridization with the Cu states, in the deep energy values, is observed, whereas in the IVA column elements of the periodic table, the s-band are so deep in energy that do not hybridize much with the rest of the electrons.

In Table VIII, we present the results for the electron distribution in the three atomic components of the noble metal series. In the second to fourth columns, we give the difference between the total number of electron of each element in the atomic case minus that number when they are alloyed. As in previous cases, Mn transfers about one electron to the other components. In the Cu series there is a modest charge transfer to Cu, except for the In and Sn alloys, cases in which Cu receives 0,73 and 0.764 electrons, respectively. In those two alloys, In and Sn transfer also electrons to the Cu atoms. In the rest of the Cu systems, the Z component also receive charge. In the Ag alloys, we have a similar behavior, except in Ag_2MnSn, in which Sn donates 0.157 electrons. In the case of the Au systems, most of the charge transfer goes to the Z element, Al, Ga, In, Si, and Ge receive more than 1 electron and Sn receives 0.452 electrons. The Au atoms donate in the cases of Z= Al, Ga, and Ge and receives electrons for Z=In, Si, and Sn.

Finally, the magnetic moments per unit cell and in each one of the components are

presented in Table IX. In column 2 we give our results and those obtained by using other theoretical methods and approximations. The experimental data is given in column 3 and is available only for the Cu systems with Z=Al, In, and Sn and Au_2MnAl. The difference between the calculated and measured values is 4.4 and 5.5 % smaller for X=Cu, Z=Al and In, respectively and 0.2 % larger for Z=Sn. One observes also that the major contribution to the magnetic moment comes from the Mn atoms and is around $4\mu_B$. Furthermore, the coupling between Mn and the other atoms is antiferromagnetic for most of the cases. In the case of Au_2MnAl there is a large discrepancy between the calculated value 3.82 μ_B and the one reported experimentally, 2.24 μ_B[2]. In the experimental measurements, performed in the sixties, they found a considerable chemical disorder in the samples. That can be a partial reason for the difference. To clarify the difference more experimental studies are needed.

The results for the magnetic moment per atomic cell as a function of the element Z, for noble metal alloys are shown in Fig. 7 c). The Cu series is plotted in yellow and acquires the lowest values, between 3.64 and 4.12 μ_B . The gold series (green curve) shows intermediate values between 3.82 and 4.22 μ_B. The largest values are attained in the Ag series, between 3.82 and 4.26 μ_B,

CONCLUSIONS

Here, we presented the most complete systematic study of the X_2MnZ Heusler alloys with X being a $3d$, $4d$, Pt, and noble metals Cu, Ag, and Au. The Z elements studied were the IIIA (Al, Si, and Ga) and IVA (Ge, In, and Sn) column elements. The spin polarized electronic structure was calculated and the energy minimized as a function of electron occupation in the spin-up and spin-down sub-bands, and the cell geometry and its size. The calculations were performed within the density functional theory using the SIESTA code. The crystalline structure and the lattice parameter agree well with the experimentally reported systems, and other theoretical results. In general, one observes an important charge transfer from the Mn atoms to the other components. The half-metallic behavior was observed only in the Fe_2MnSi, Co_2MnSi, and Ru_2MnGe alloys. From the electronic structure, the most promising alloys for spintronic applications is Fe_2MnSi. Furthermore, we found that the highest magnetic moment per unit cell (7.86 μ_B) is obtained in the Fe_2MnIn and the smallest

($2.15\mu_B$) in Ru_2MnAl. In general, our theoretical results for the magnetic moment per unit cell agree very well with those measured experimentally, and other theoretical results.

ACKNOWLEDGMENTS

We acknowledge comments and discussions with Andrés Vega and Luis Carlos Balbás from the Universidad de Valladolid (Spain). R.H.A.T acknowledges financial support from CONACyT Mexico, scholarship 415121 and the financial support of the Universidad de Valladolid (Spain). We also acknowledge to J. Limón from the Computer Center of the IF-UASLP for computational support in all the calculations.

* faustino@ifisica.uaslp.mx; aguilera_rodrigo123@hotmail.com

† joseluis.moran@ipicyt.edu.mx

[1] Heusler F 1903 *Verh. Dtsch. Phys. Ges.*, **5**, 219

[2] Oxley DF, Tebble RS, and Williams FC 1963 *J. Appl. Phys.*, **34**, 1362

[3] Webster PJ 1969 *Contemp. Phys.* **10**, 559

[4] Hames FA and Crangle J 1971 *J. Appl. Phys.*, **42**, 1336

[5] Campbell CCM, 1975 *J. Phys. F*, **5**, 1931

[6] Webster PJ, Ziebeck KRA. Town SL, and Peak MS, 1984 *Phil. Mag. B*, **49** 295

[7] Ziebeck KRA and Webster PJ, 1984 *J. Phys. F*, **5**, 1756

[8] Cadeville MC and Morán-López JL 1987 *Phys. Rep.* **153**, 331

[9] Morán-López JL, Rodríguez-Alba R, and Aguilera-Granja F 1994 *J. Magn. Magn. Mater.*, **131**, 417

[10] Planes A, Mañosa L, and Acet M 2009 *J. Phys. Condens. Matter* **21** 233201

[11] Palmstrom C 2003 *MRS Bull.* **28**, 725

[12] Picozzy S 2008 *Adv. Solid State Phys.*, **47**, 129

[13] Ullakko K, Huang JM, Kantner C, O'Handley RC, and Kokorin VV 1996 *Appl. Phys. Lett.*, **69**, 1966

[14] Ishida S, Ishida J, Asano S, and Yamashita J. *J. Phys. Soc. Japan*, **45**, 1239 (1978)

[15] Ishida S, Akasawa S, Kubo Y, and Ishida J, *J. Phys. F Met. Phys*, **12** 1111 (1982)

[16] Kübler J, Williams AR, and Sommers CB, *Phys. Rev. B*, **28**, 1745 (1983)

[17] Fujii S, Ishida S, and Asano S, *J. Phys. Soc. Jap.*, **58**, 3657 (1989)

[18] Ayuela A, Enkovaara J, Ullakko K, and Nieminen EM, *J. Phys. Cond. Matter*, **11**, 2017 (1999)

[19] Deb A and Fakurai Y, *J. Phys. Cond. Matter*, **12**, 2997 (2000)

[20] Kulkova SE, Eremeev, SV, Kulkov SS, *Solid State Comm.*, **130**, 793 (2004)

[21] Kulkova SE, Kulkov SS, and Subashiev AV, *Comp. Mat. Sci.*, **36**, 249 (2006)

[22] Godlevsky VV and Rabe KM, *Phys. Rev. B*, **63**, 134407 (2001)

[23] Şaşioğlu E, Sandratskii LM, and Bruno P, *Phys. Rev. B*, **70**, 024427 (2004)

[24] Soler JM, Artacho E, Gale JD, García A , Junquera J, Ordejón F, and Sánchez-Portal D 2002 *J. Phys. Condensed Matter* **14**, 2745

[25] Perdew JP, Burke K, and Ernzerhof M 1996 *Phys. Rev. Lett.* **77**, 3865

[26] Troullier N, and Martins JL 1991 *Phys. Rev. B* **43**, 1993

[27] Kleinman L and Bylander MD 1982 *Phys. Rev. Lett.* **48**, 1425

[28] Aguilera-Granja F, García-Fuente A, and Vega A 2008 *Phys. Rev. B*, **78**, 134425

[29] Aguilera-Granja F, Piotrowski MJ, and da Silva JL 2013 *Euro. Phys. J. D*, **67**, 33

[30] Press WH, Teukolsky SA, Vetterling WT, and Flannery BP 1992 *Numerical Recipes in Fortran* (Cambridge University Press, Cambridge, 2nd Ed.)

[31] Niculescu V, Burch TJ, Raj K, and Budnick JL 1977 *J. Magn. Mag. Mat.*, **5**, 60

[32] Kim RJ, Lee NN, Kim BJ, Lee YP, Kudryavtsev, and Kim KW 2015 *IEEE, Trans. Magnetics*, **41** 3443